Hybrid lipid-AuNP clusters as highly efficient SERS substrates for biomedical applications

Authors: Jacopo Cardellini*, Caterina Dallari*, Ilaria De Santis, Lorenzo Riccio, Costanza Ceni, Amelia Morrone, Martino Calamai, Francesco Saverio Pavone, Caterina Credi, Costanza Montis, Debora Berti

Supplementary Figures

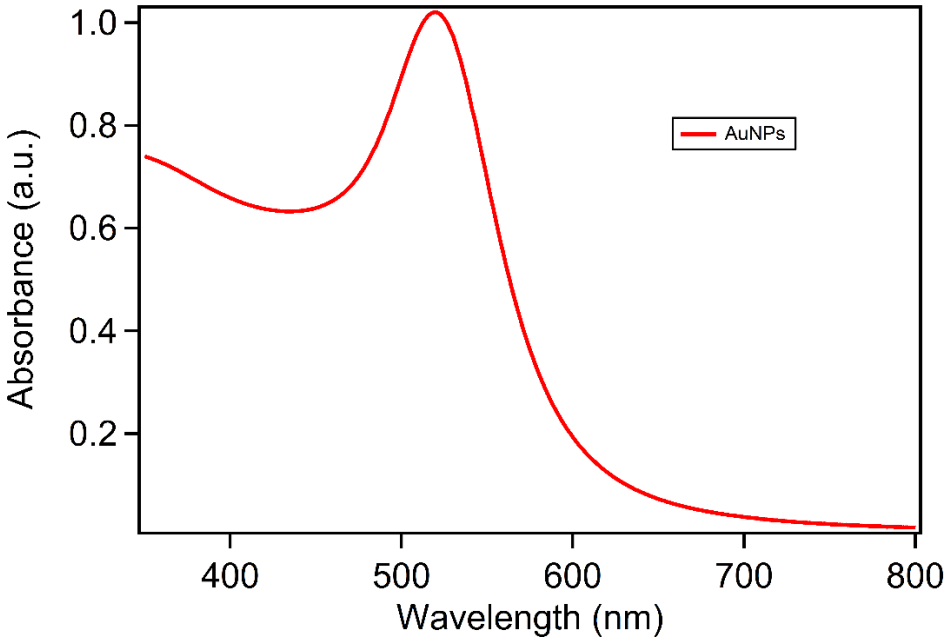

Supplementary Figure 1. **Characterization of AuNPs: UV-vis spectroscopy.** *UV-Vis absorption spectrum of AuNPs collected between 350 nm and 800 nm.*

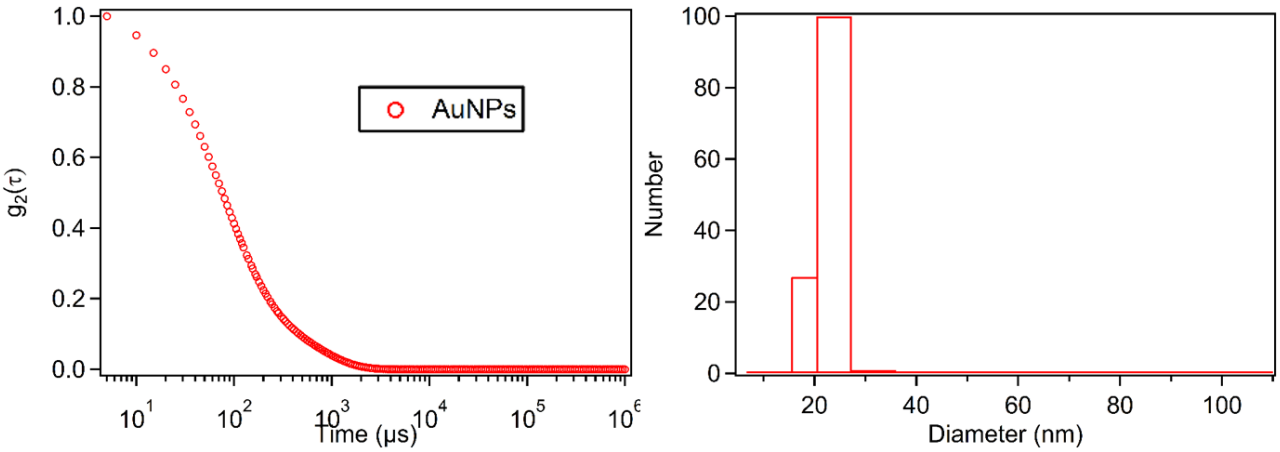

Supplementary Figure 2. Characterization of AuNPs: DLS. *Dynamic Light Scattering measurements of AuNPs.* The AuNPs hydrodynamic diameter and surface potential in MilliQ water were evaluated through Dynamic Light Scattering and Zeta-Potential, respectively, and reported in Supplementary Table 1. The evaluated hydrodynamic diameter is consistent with the UV-vis analysis reported in Supplementary Note 1.

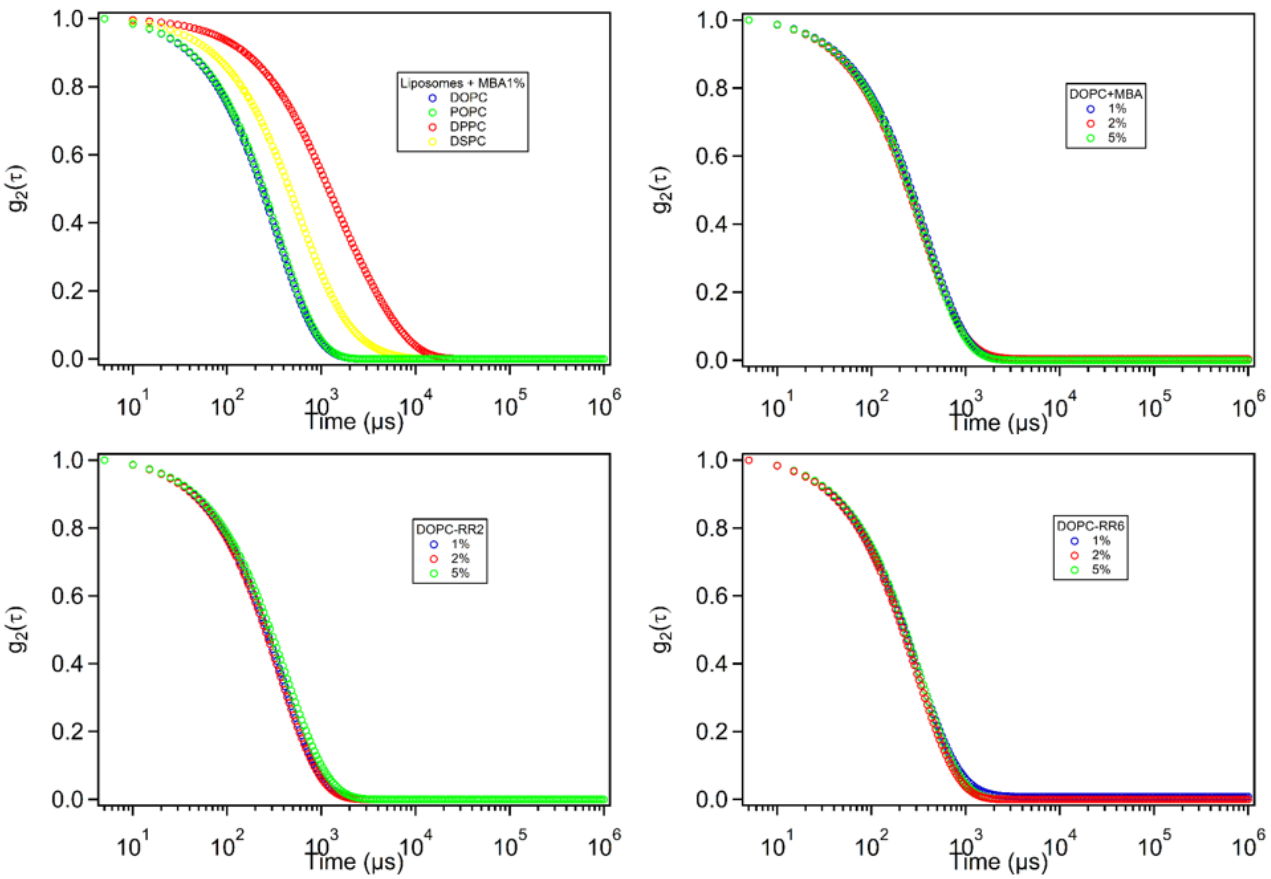

Supplementary Figure 3. **Characterization of Liposomes: DLS.** *Normalized autocorrelation functions of a) DOPC, POPC, DPPC, and DSPC liposome dispersions encapsulating 1% of MBA, b) DOPC liposomes containing 1%, 2%, and 3% MBA (w/w), c) DOPC liposomes containing 1%, 2%, and 3% RR2, and d) DOPC liposomes containing 1%, 2%, and 3% RR6.* The hydrodynamic dimensions of the different liposomes are obtained through Dynamic Light Scattering. In Supplementary Figure 3 the normalized DLS curves of the liposome are reported. The average hydrodynamic diameters evaluated for DOPC and POPC liposomes are 104 nm (PDI 0.1) and 107 nm (PDI 0.1), respectively, while DPPC and DSPC have an average hydrodynamic size of 150 nm (PDI 0.2) and 125 nm (PDI 0.2). As shown by the superimposition of the normalized autocorrelation functions in panels b, c, and d, variations in the Raman reporter concentration do not significantly affect the liposomal size.

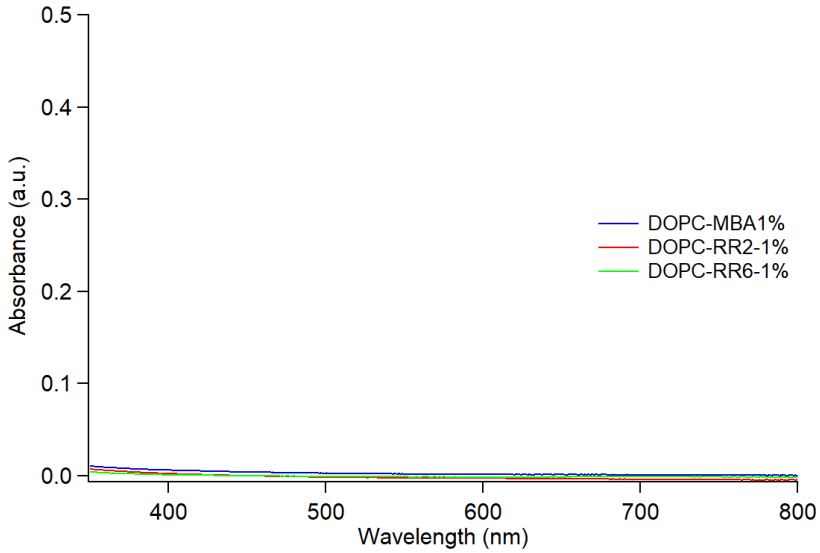

Supplementary Figure 4. Characterization of Lipsomes: UV-vis spectroscopy. *UV-visible spectra of 1.2 nM DOPC(MBA), DOPC(RR2), and DOPC(RR6) dispersions.* UV-visible spectra of liposomal dispersions were acquired. As shown the dispersions do not have any significant signal in the visible region (350-800 nm) in the absence of AuNPs.

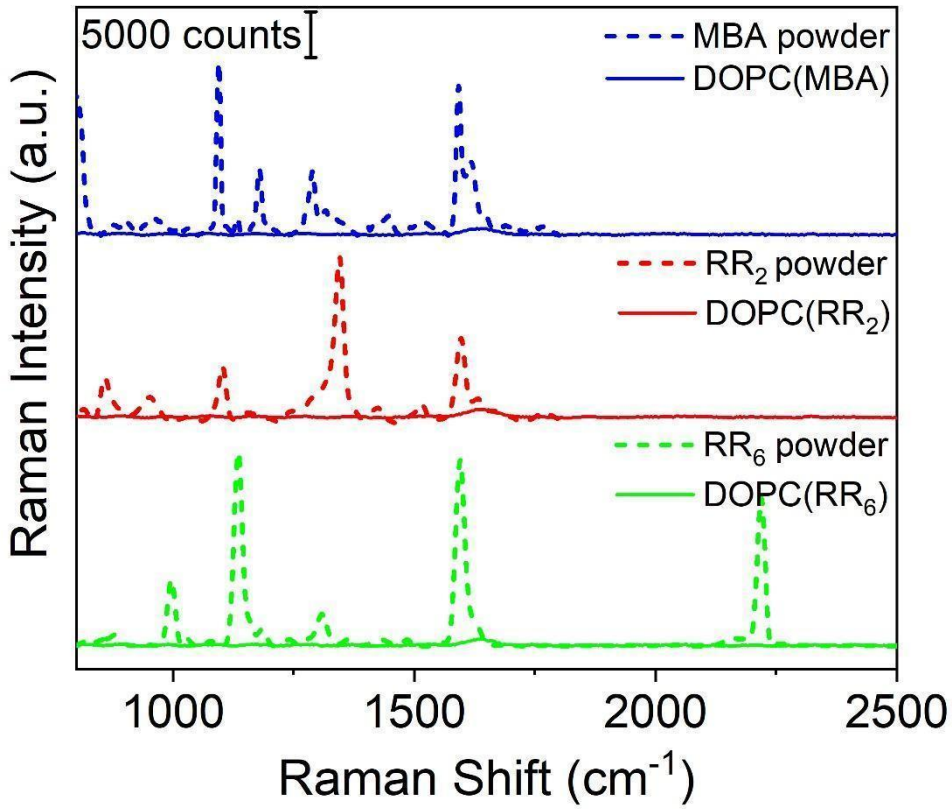

Supplementary Figure 5. Characterization of liposomes and RRs: Raman spectroscopy. *Raman spectra of different RR (MBA, RR2, and RR6) powders (dotted lines) and of the same RRs conjugated with DOPC liposomes (1.2 nM, continue lines).* The Raman spectrum of DOPC liposomes containing MBA, RR2, and RR6 were acquired, showing that in the absence of AuNPs any Raman signal can be detected in the dispersions.

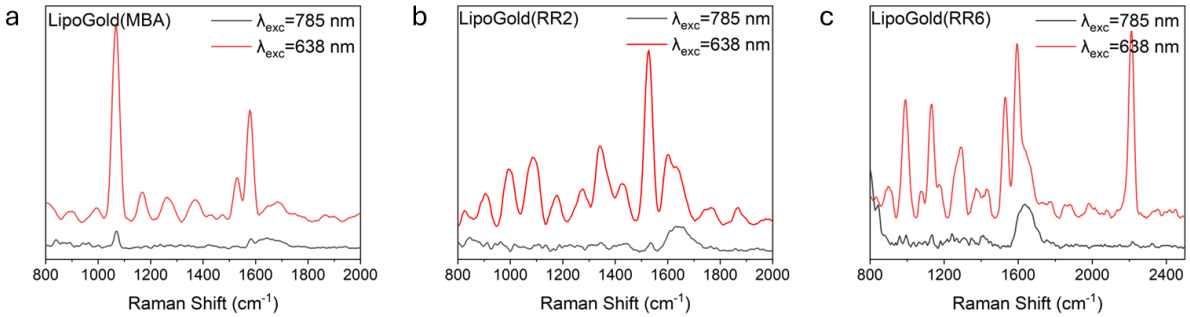

Supplementary Figure 6. Effect of laser wavelength in Raman spectra. Raman spectra of DOPC liposomes containing MBA (a), RR2 (b), and RR6 (c) acquired with different laser wavelengths (638 and 785 nm), keeping constant all the working parameters.

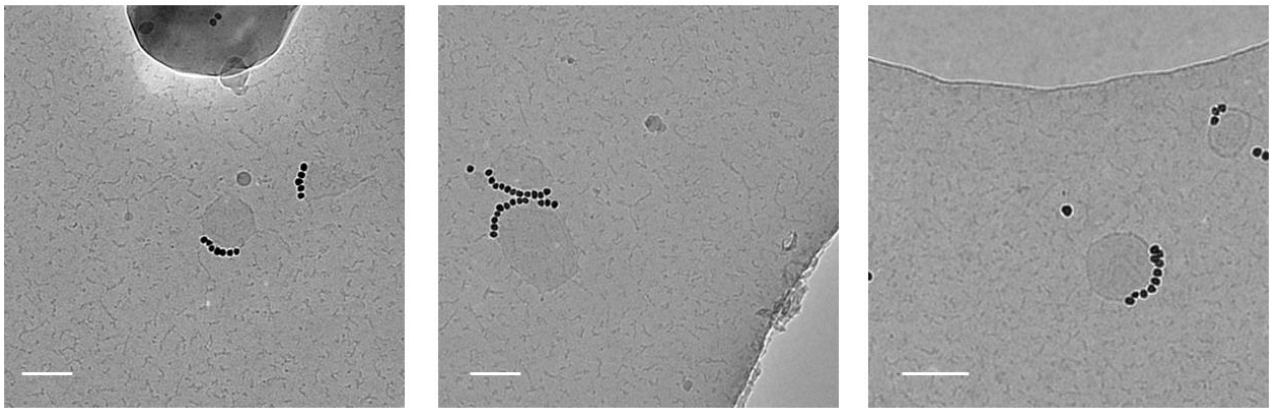

Supplementary Figure 7. Morphology of AuNPs-DOPC hybrids. *Cryo-EM images of DOPC(MBA)-AuNPs composites (scale bars 100 nm).*

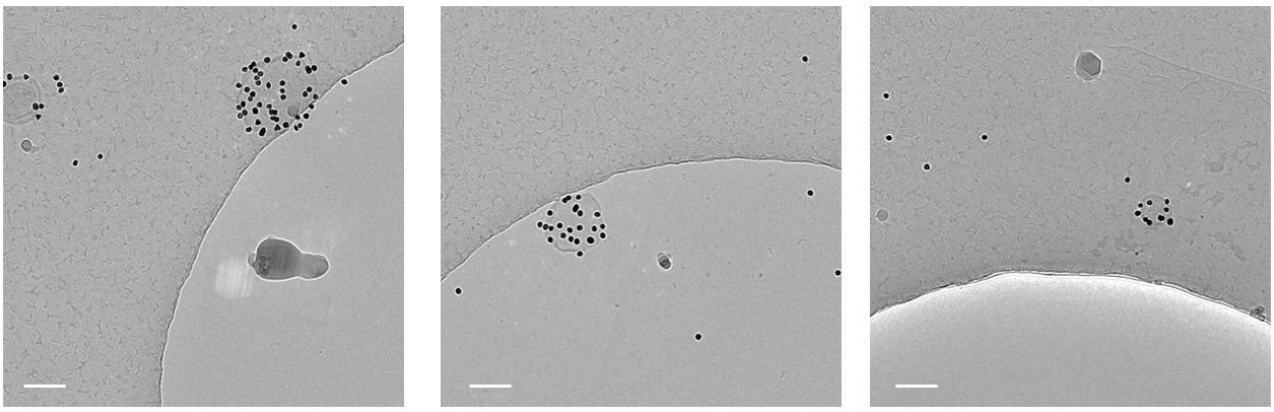

Supplementary Figure 8. Morphology of AuNPs-DPPC hybrids. *Cryo-EM images of DPPC(MBA)-AuNPs composites (scale bars 100 nm).*

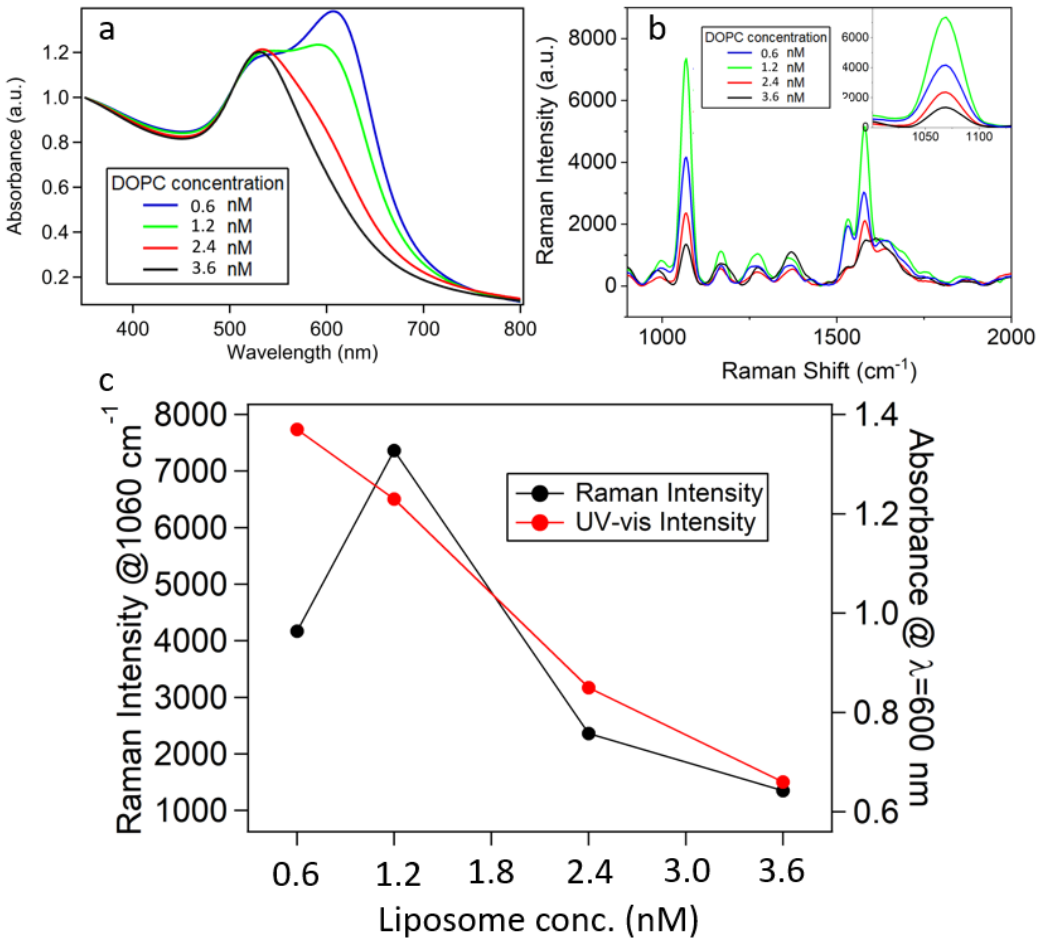

Supplementary Figure 9. Optimization of SERS signal: DOPC(MBA)-AuNPs. *a) UV-visible spectra of AuNPs interacting with liposome dispersion of DOPC(MBA) at different concentrations; b) Raman spectra of AuNPs interacting with liposome dispersion of DOPC(MBA) at different concentrations; c) Variations of Raman intensity at 1060 cm^{-1} and absorbance intensity at 600 nm as a function of liposome concentration. UV-Visible and Raman-SERS spectra of different quantities of*

DOPC liposomes containing MBA were acquired. As shown in panel a), the aggregation of AuNPs increases as the liposome concentration decreases. This experimental evidence can be explained by considering that the increase in the number of particles per liposome leads to larger and more compact AuNPs clusters. However, as shown in panel b, on the other hand, a decrease in the liposome concentration results in a simultaneous decrease of the overall MBA concentration. The overall amount of MBA and the DOPC concentration dictate the AuNPs aggregation and SERS Enhancement and need to be balanced. As shown in panel c, the optimal conditions to maximize the SERS signals of MBA taking into account both MBA concentration and AuNPs aggregation are obtained for a DOPC concentration of 1.2 nM.

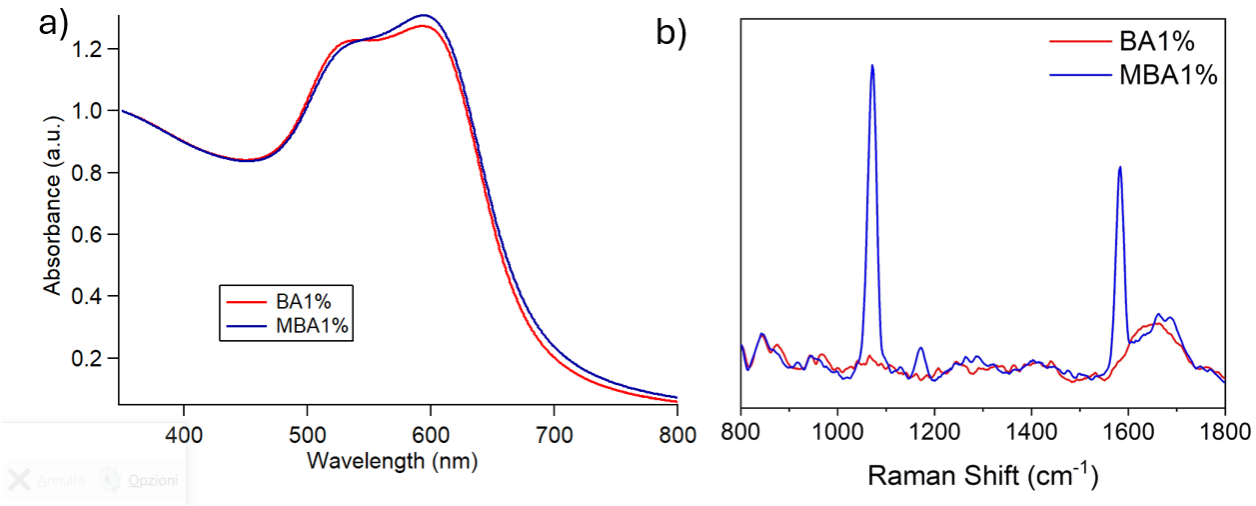

Supplementary Figure 10. Effect of thiolated moieties in the SERS enhancement of MBA-DOPC tags. UV-vis (a) and Raman (b) spectra of AuNPs interacting with liposomes embedding MBA (blue curves) and BA (red curves). To prove that the SERS enhancement can be attributed to a close interaction between MBA and AuNPs, driven by the MBA thiol pendant group, we compared plasmonic and Raman signal arising from AuNPs clustered on DOPC liposome encapsulating Mercaptobenzoic acid (MBA) and benzoic acid (BA) that can be distinguished only for the thiol moiety. Liposomes containing benzoic acid (BA) were prepared and plasmonic and Raman variations after the AuNPs aggregation were monitored. As shown in the figures, since the plasmonic spectra are not dramatically affected by the presence of the thiolated molecules, while the Raman signal for BA-containing liposomes disappears, we can hypothesize that the enhanced Raman signals arise from the interaction between thiol moieties and AuNPs."

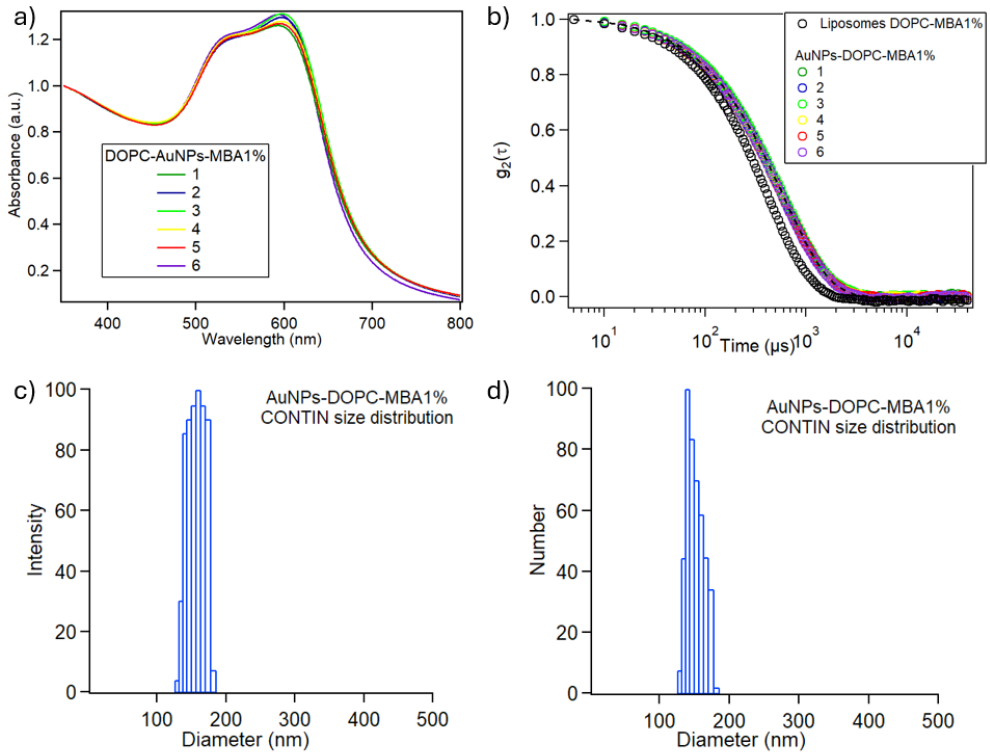

Supplementary Figure 11. Plasmonic and size reproducibility of DOPC(MBA)-AuNPs. (a) UV-vis spectroscopy of 6 different of DOPC(MBA)-AuNPs hybrids; (b) DLS autocorrelation functions of 6 different of DOPC(MBA)-AuNPs hybrids and DOPC(MBA) liposomes with black dashed line representing the Contin fitting; Size distributions based on scattering intensity (c) and particle number (d) of DOPC(MBA)-AuNPs hybrids from CONTIN analysis. The reproducibility of DOPC(MBA)-AuNPs suprastructures was additionally assessed by comparing plasmonic variations and particle size of six different batches after 30 minutes of incubation of AuNPs with DOPC(MBA) liposomes via UV-vis spectroscopy and DLS analysis. As shown in panels a) and b), plasmonic and DLS variations are minimal. The autocorrelation curves have been fitted through a Contin algorithm and the size distribution has been shown both weighted on scattering intensity and particle number (panels c) and d) respectively). The analysis shows the presence of a single-size population peaked at about 150 nm (size consistent with the size of liposomes with a AuNPs crust).

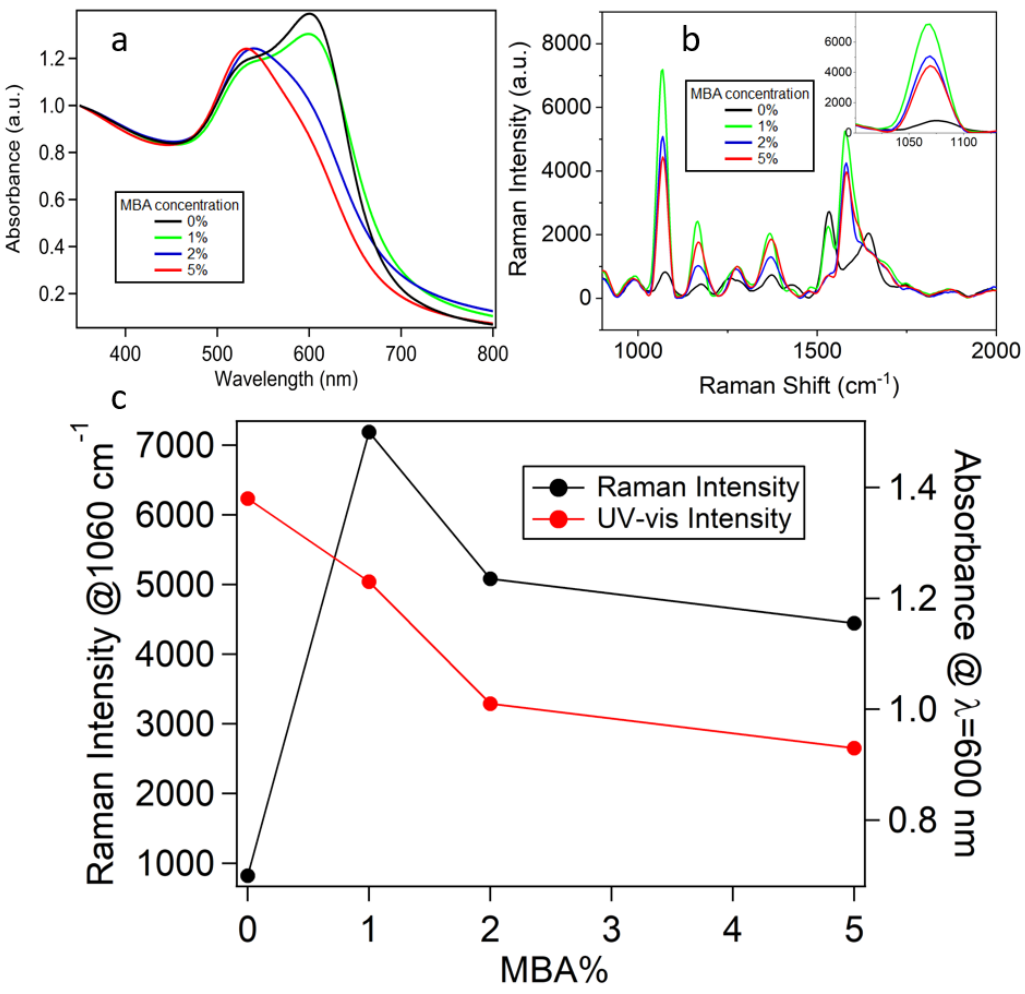

Supplementary Figure 12. Effect of MBA concentration. a) UV-visible spectra of AuNPs interacting with DOPC liposome dispersion with different MBA concentrations; b) Raman spectra of AuNPs interacting with AuNPs interacting with DOPC liposome dispersion with different MBA concentrations; c) Variations of Raman intensity at 1060 cm^{-1} and absorbance intensity at 600 nm as a function of MBA concentration. UV-Visible and Raman-SERS spectra of liposomes containing different quantities of MBA were acquired, showing that the best condition in terms of SERS enhancement is for 1% MBA (mol/mol). As shown in panel a, the increase of the MBA concentration per liposome provokes a decrease in the AuNPs aggregation. This behavior can be rationalized according to the interaction mechanism hypothesized in our recent publications. Briefly, the aggregation of AuNPs is driven by a ligand exchange, occurring between the citrate molecules originally adsorbed to the AuNP surface and the polar heads of lipids upon the AuNP docking on the liposomal membrane. The citrate is released from the gold surface due to the AuNP docking, provoking a local and transient increase of the ionic strength which triggers the clustering of other neighboring AuNPs. The amount of citrate released depends on the wrapping of the membrane around the AuNPs as the higher the surface contact between the AuNP and the liposomal surfaces, the higher the citrate released. As we recently demonstrated, the membrane rigidity, which dramatically affects the extent of wrapping, governs the citrate release and the AuNPs clustering. According to this interaction mechanism, the decrease of AuNPs aggregation

with increasing the MBA concentration can be explained considering that: a) the increase of the MBA concentration within the membrane induces a decrease in the membrane fluidity, reducing the wrapping extent and, thus, the citrate release; b) the thiolate moieties in the Raman Reporter structure covalently bond the gold surface, altering membrane wrapping and citrate-lipid ligand exchange.

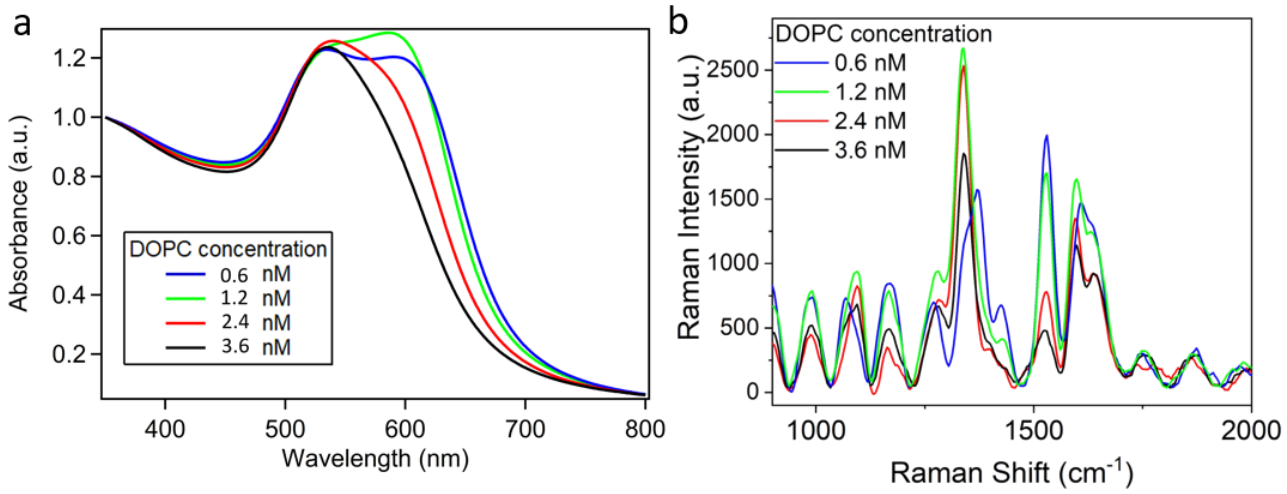

Supplementary Figure 13. Characterization of DOPC(RR2)-AuNPs composites: effect of DOPC concentration. *a) UV-visible spectra of AuNPs interacting with liposome dispersion of DOPC(RR2) at different concentrations; b) Raman spectra of AuNPs interacting with liposome dispersion of DOPC(RR2) at different concentrations. UV-Visible and Raman-SERS spectra of different quantities of DOPC liposomes containing RR2 were acquired, showing that the best condition in term of SERS enhancement is DOPC 1.2 nM.*

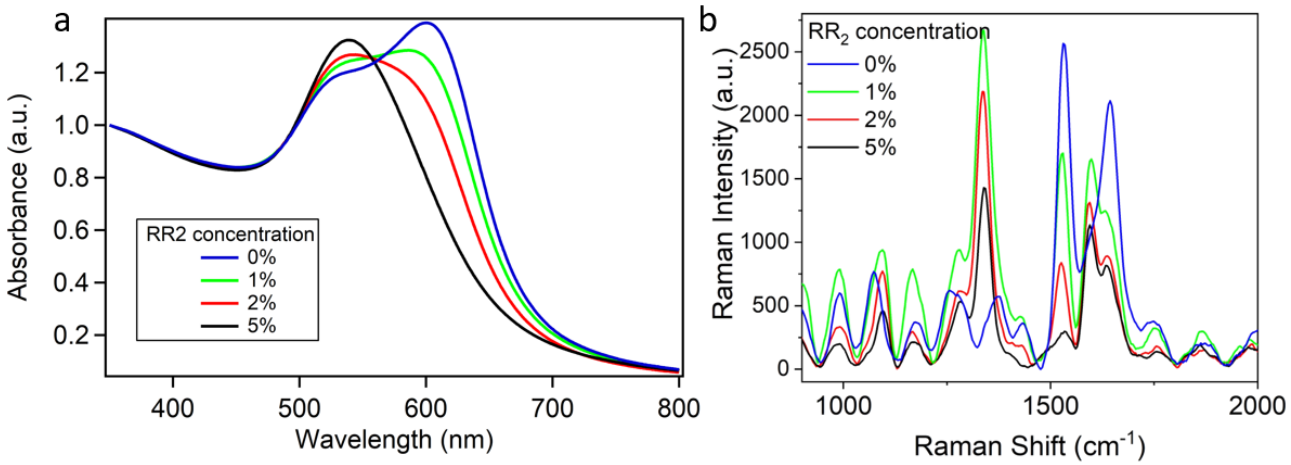

Supplementary Figure 14. Characterization of DOPC(RR2)-AuNPs composites: effect of RR2 concentration. *a) UV-visible spectra of AuNPs interacting with DOPC liposome dispersion with*

different RR2 concentrations; b) Raman spectra of AuNPs interacting with AuNPs interacting with DOPC liposome dispersion with different RR2 concentrations. UV-Visible and Raman-SERS spectra of liposomes containing different quantities of RR2 were acquired, showing that the best condition in term of SERS enhancement of the signal at 1340 cm-1 is 1% RR2 (green curve).

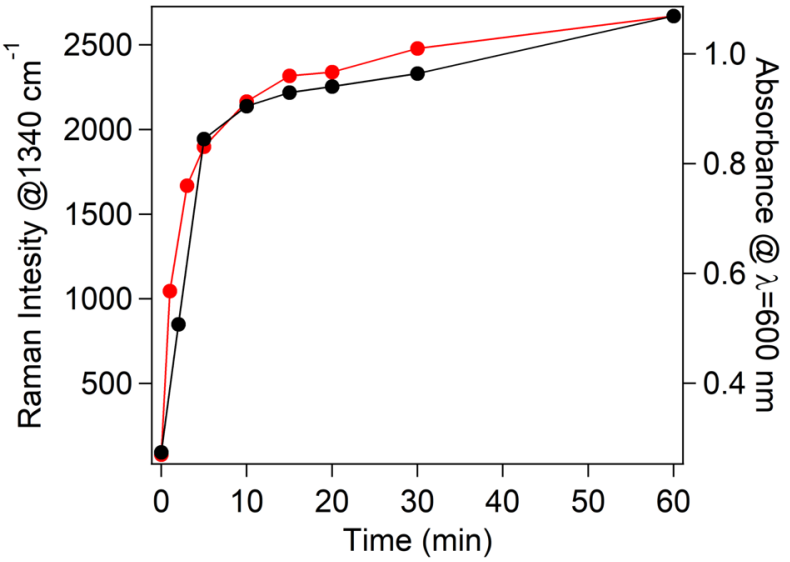

Supplementary Figure 15. Characterization of DOPC(RR2)-AuNPs composites: Raman and UV-vis time evolution. *DOPC(RR2) liposome interacting with AuNPs, comparison between the time evolution of Raman Intensity at 1340 cm-1 and UV-vis signal at 600 nm.*

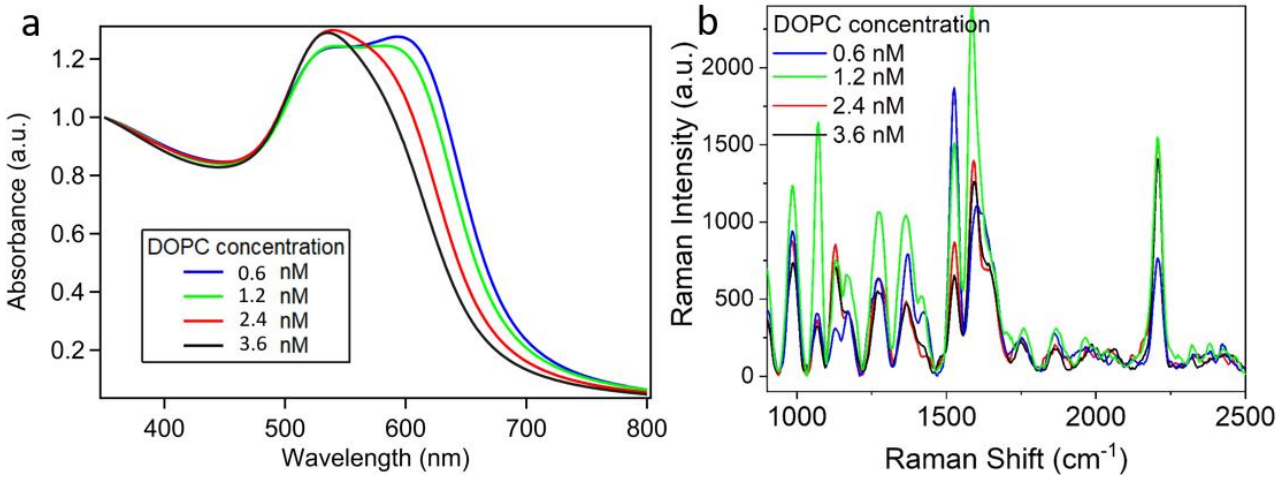

Supplementary Figure 16. Characterization of DOPC(RR6)-AuNPs composites: effect of DOPC concentration. *a) UV-visible spectra of AuNPs interacting with liposome dispersion of DOPC(RR6) at different concentrations; b) Raman spectra of AuNPs interacting with liposome dispersion of DOPC(RR6) at different concentrations. UV-Visible and Raman-SERS spectra of different quantities of DOPC liposomes containing RR6 were acquired, showing that the best condition in terms of SERS*

enhancement of the signal peaked at 2210 cm-1 is DOPC 1.2 nM.

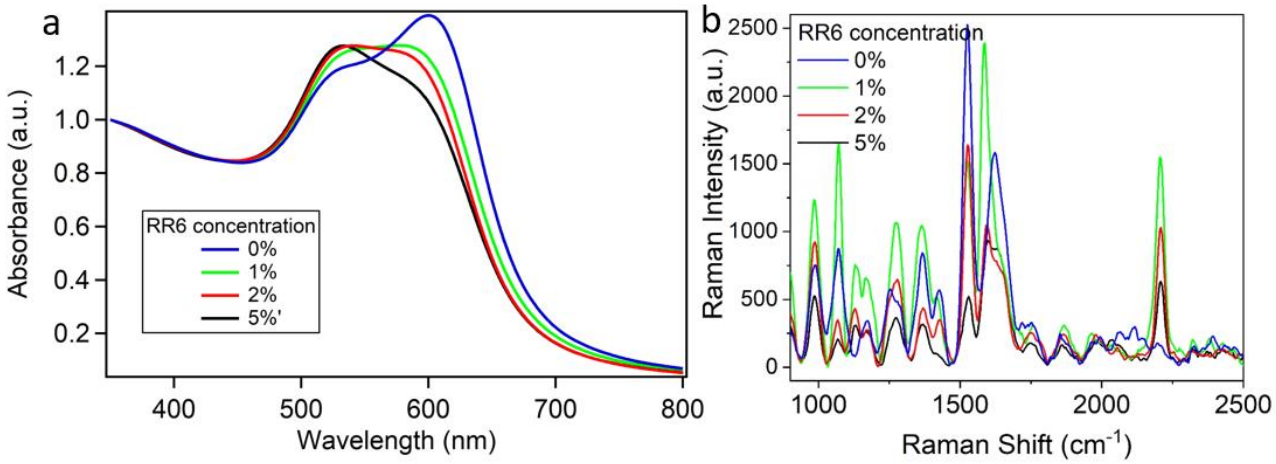

Supplementary Figure 17. Characterization of DOPC(RR6)-AuNPs composites: effect of RR6 concentration. *a) UV-visible spectra of AuNPs interacting with DOPC liposome dispersion with different RR6 concentrations; b) Raman spectra of AuNPs interacting with AuNPs interacting with DOPC liposome dispersion with different RR6 concentrations. UV-Visible and Raman-SERS spectra of liposomes containing different quantities of RR6 were acquired, showing that the best condition in term of SERS enhancement is 1% RR6.*

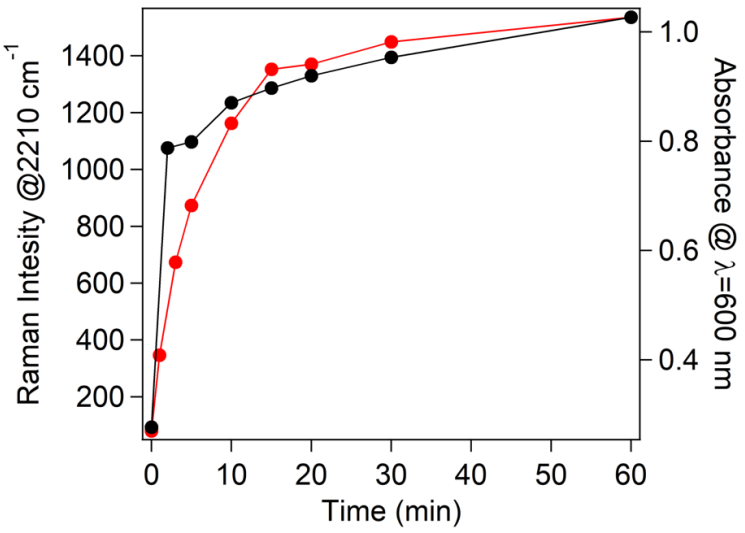

Supplementary Figure 18. Characterization of DOPC(RR6)-AuNPs composites: Raman and UV-vis time evolution. *DOPC(RR6) liposome interacting with AuNPs, comparison between the time evolution of Raman Intensity at 2210 cm-1 and UV-vis signal at 600 nm.*

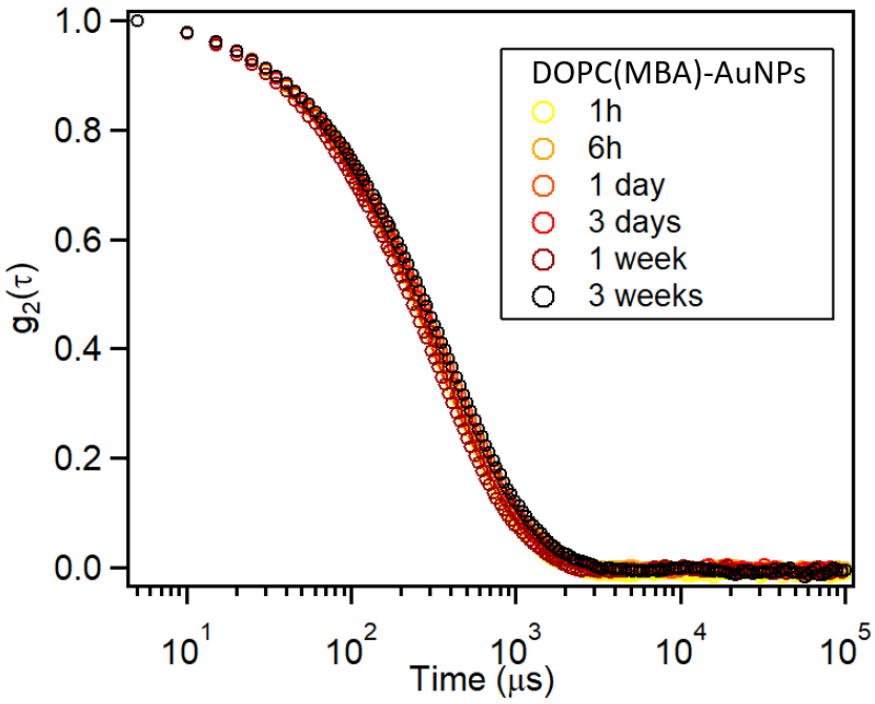

Supplementary Figure 19. Time evolution of DOPC(MBA)-AuNPs composites. *Normalized autocorrelation functions of DOPC(MBA)-AuNPs dispersions collected up to 3 weeks of interaction.*

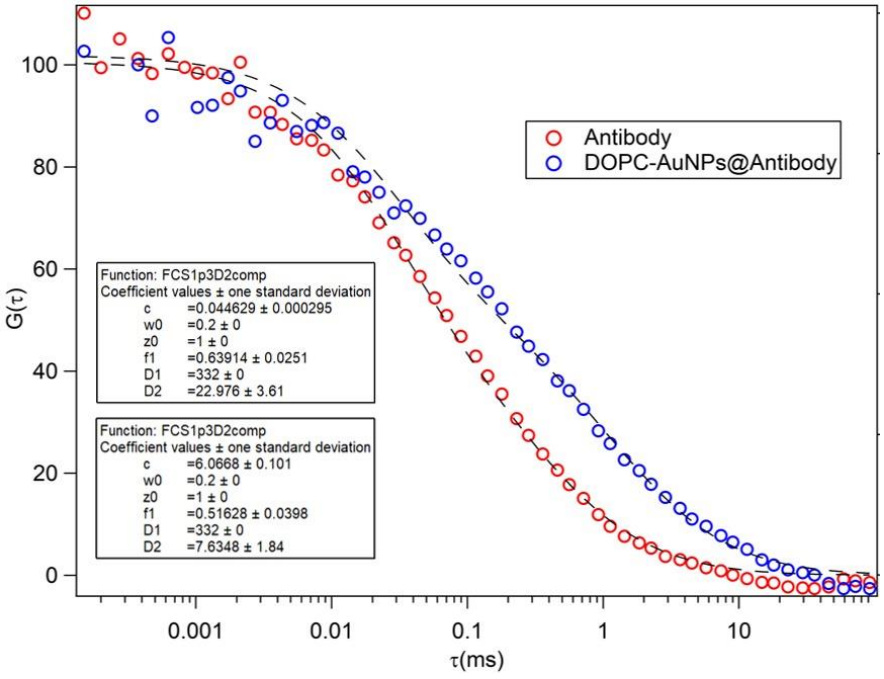

Supplementary Figure 20. Bioconjugation of LipoGold tags. *Fluorescence correlation spectroscopy (FCS) measurements of antibodies (Ab(I)) (red circles) and DOPC-AuNPs@antibody conjugates (blue circles). The fitting parameters of the black dashed lines are reported in the image. See supplementary note 3 for further information.*

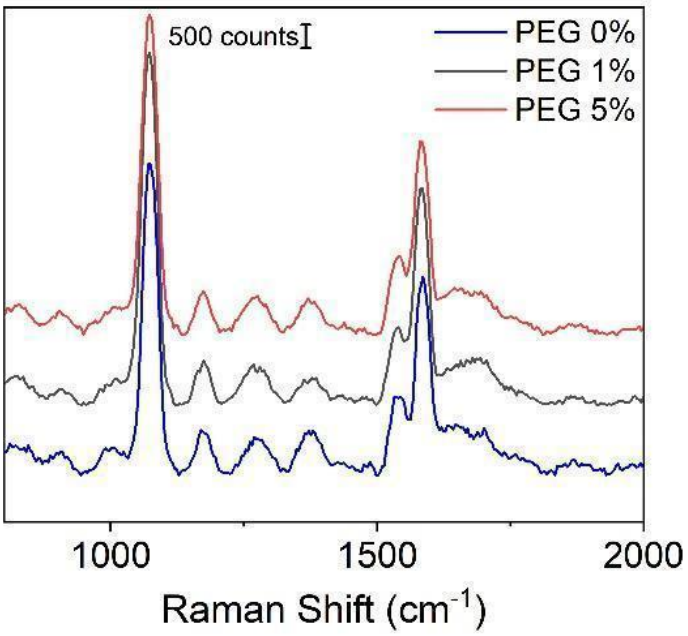

Supplementary Figure 21. Effect of the percentage of pegylated lipids on SERS signals of LipoGold tags. *Raman-SERS spectra of AuNPs-DOPC(4-MBA) varying the quantity of PEG from 0% to 5%. Raman-SERS spectra of DOPC liposomes containing MBA functionalized with different quantities of DOPE-PEG were acquired, showing that no variation in term of Raman signal intensity was experienced for all conditions.*

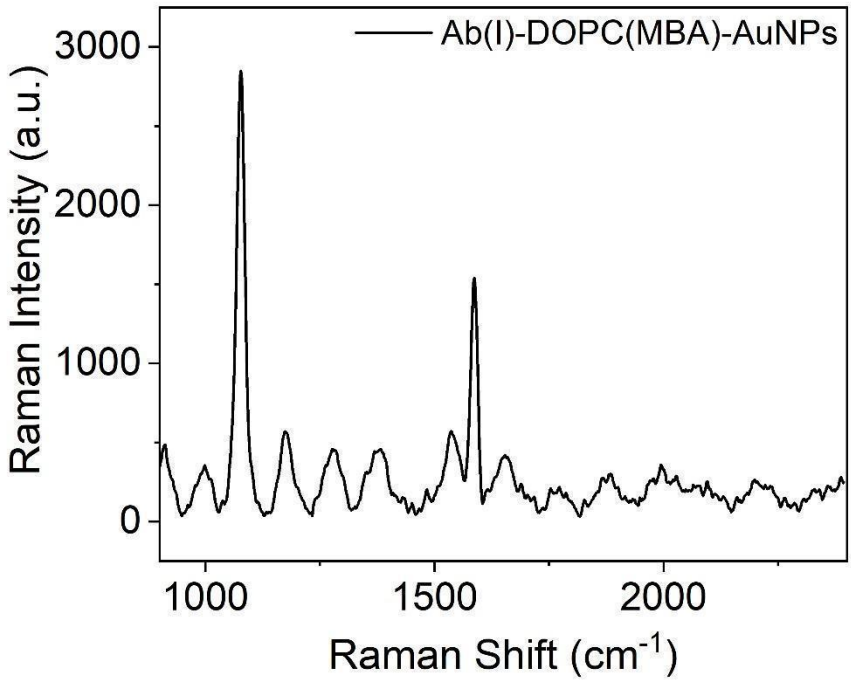

Supplementary Figure 22. SERS signal of LipoGold tags after bioconjugation. *Raman-SERS spectra of Ab(I)-DOPC(4-MBA)-AuNPs.*

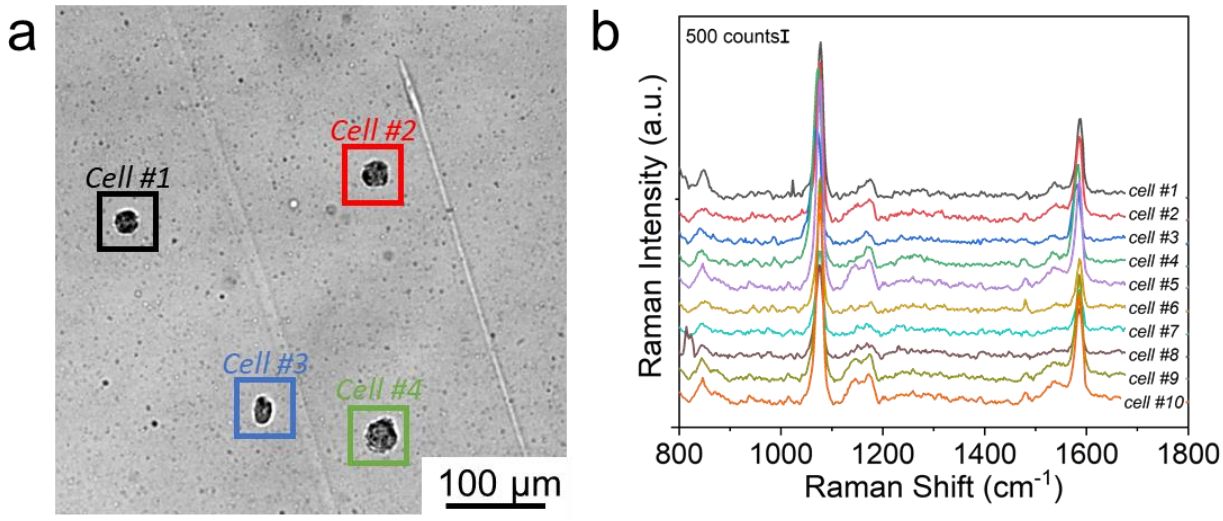

Supplementary Figure 23. LipoGold tags targeting cells. *a) Wide-field image of deposited patient cells on CaF_2 substrate, after their detachment with trypsin, fixation and permeabilization; b) Raman-SERS spectra acquired from 10 individual cells of patient sample.*

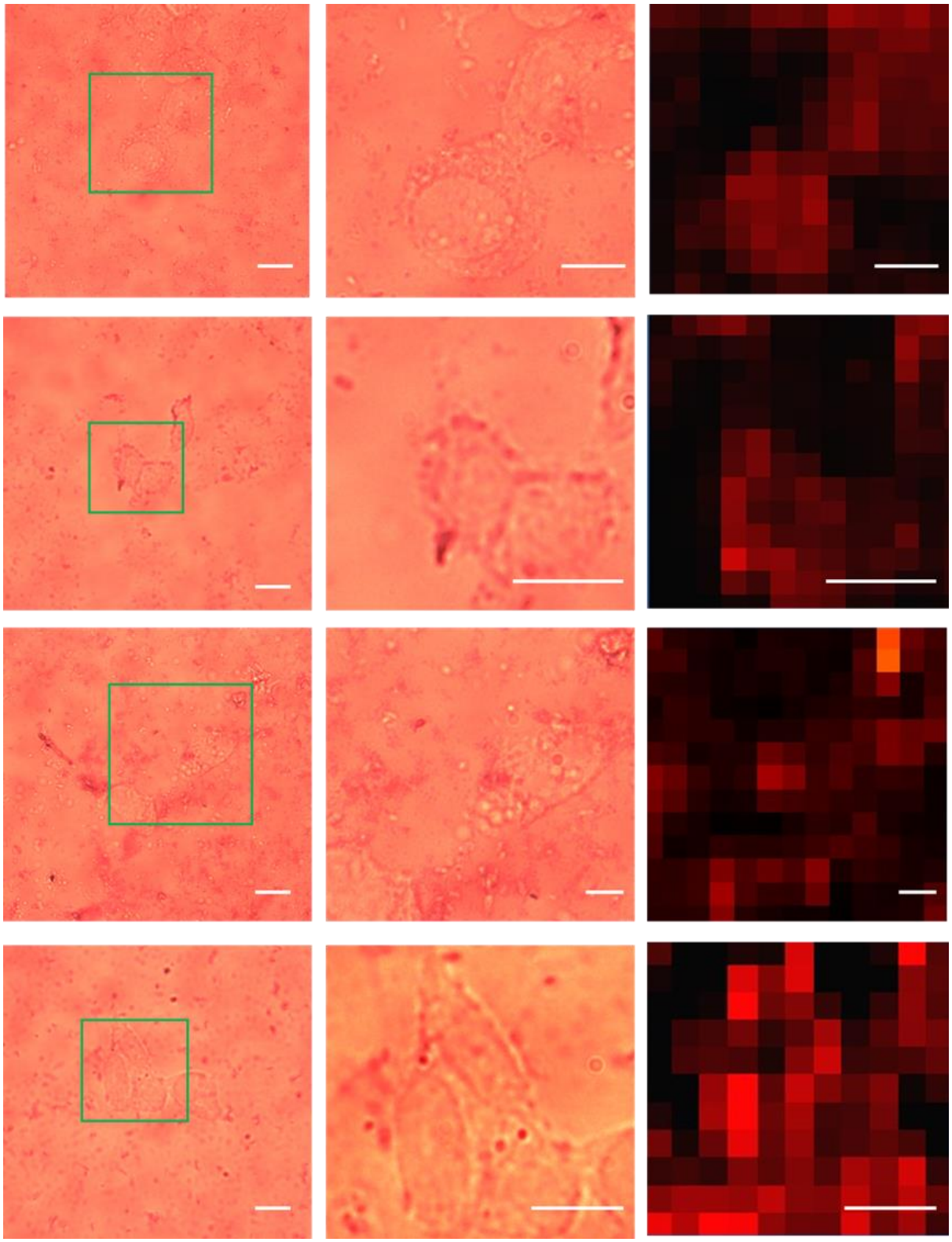

Supplementary Figure 24. Raman maps of cells labeled with LipoGold tags. *Bright-field images of the analysed SH-SY5Y cells treated with LipoGold(RR6) for 90 min. The green rectangle represents the scanned area with Raman confocal microscopy. Zoomed bright field images of the scanned area. SERS maps built exploiting the intensity at 2210 cm-1. Scalebar is 10 um in all cases*

Supplementary Tables

	D_h (nm)	Z-Potential (mV)
AuNPs	22 ± 2	-32 ± 5

Supplementary Table 1. AuNPs characterization. *Hydrodynamic diameter obtained from cumulant analysis of Dynamic Light Scattering curve and Zeta Potential values of AuNPs.*

LIPOSOME	Hydrodynamic Size	Concentration
DOPC	104 (PDI 0.1)	38 nM
POPC	107 (PDI 0.1)	42 nM
DPPC	150 (PDI 0.2)	15 nM
DSPC	125 (PDI 0.2)	20 nM

Supplementary Table 2. Liposome Characterization. *Hydrodynamic diameters obtained from cumulant analysis of Dynamic Light Scattering curve and concentration values of DOPC, POPC, DPPC, and DSPC water dispersions. The starting lipid concentration of DOPC, POPC, DPPC and DSPC water dispersions was 4 mg/mL. The liposome concentrations in the final dispersions were then evaluated from the hydrodynamic diameter of each liposomal batch. First, the liposomal surface area (surface area=$4\pi r^2$) was calculated from the liposome diameters. Then, the doubled surface was divided by the lipid cross-section (0,5 nm^2) in order to obtain the lipid number per liposome, considering that, as the bilayer thickness (about 4-5 nm) is negligible with respect to the liposomes' average diameter, the same number of lipid molecules localizes in the internal and external monolayers. The total number of lipids was divided by the calculated number of lipids per vesicle, obtaining the number of vesicles. Finally, the number of vesicles was divided for the Avogadro constant N_A and multiplied by the dispersion volume. The obtained molar concentrations of the vesicles are reported in the table.*

Supplementary Notes

Supplementary Note 1

We evaluated the AuNPs size via UV-Vis spectroscopy by exploiting the following equation:

$$d = exp\,(B_1 \frac{A_{spr}}{A_{450}} - B_2)$$

with d diameter of gold nanoparticles, A_{spr} absorbance at the surface plasmon resonance peak, A_{450} absorbance at 450 nm and B_1 and B_2 are dimensionless parameters, taken as 3 and 2,2, respectively. The diameter value obtained is 12 nm.

Then, the concentration of AuNPs was determined with the Lambert-Beer law ($E(\lambda) = \varepsilon(\lambda)lc$), taking the extinction values $E(\lambda)$ at the LSPR maximum, i.e. λ = 520 nm. The extinction coefficient $\varepsilon(\lambda)$ of AuNPs was determined by the Wang method, by the following equation:

$$ln\,(\varepsilon) = kln(d) + a$$

with d core diameter of nanoparticles, and k and a dimensionless parameters ($k = 3{,}32111$ and $a = 10{,}80505$). The final concentration of the citrate-capped AuNPs is therefore ~ $6.2 \cdot 10^{-9}$ M.

Supplementary Note 2

The formula used to calculate the enhancement factor (EF) is as follows:

$$EF = \frac{I_{SERS}}{I_{Raman}} \times \frac{C_{Raman}}{C_{SERS}}$$

Where:

I_{SERS} is the intensity of the SERS peak calculated for LipoGold tags; I_{Raman} is the intensity of the Raman peak of the RR molecules dispersed in solution; C_{Raman} and C_{SERS} are the concentrations of the RR molecules in solution and in LipoGold tags, respectively.

Supplementary Note 3

Fluorescence Correlation Spectroscopy:

To go further in detail, the FCS curves were fitted with a multimodal distribution of two populations, as a single decay time cannot describe the profile of the autocorrelation functions, according to the following equation:

$$G(\tau) = 1/N(1 + \frac{\tau}{\tau D})^{-1}(1 + \frac{\tau}{S^2 \tau D})^{-1/2}$$

where N indicates the average number density of the fluorescent objects, w0, and z0 are experimentally determined structural parameters of the detection molecules, D1 and D2 are the diffusion coefficients of the fluorescent colloidal objects, and f1 is the weight factor of each diffusing component of the decay time. Concerning the free antibody (red circles in Figure 5b) 1) represents the diffusion coefficient of the free dye probably not bound to the antibody, and 2) represents the diffusion coefficient of the labeled antibody and corresponds to a hydrodynamic size of about 10 nm. After the coupling of the antibody to AuNPs-liposome adducts, the lowest diffusion coefficient 2) further decreases, indicating the binding of the antibody to the pegylated lipids of the liposomal bilayer. The hydrodynamic diameter extrapolated from the fitting (50 nm) is intermediate between the size of the antibody (10 nm) and the size of the AuNPs-DOPC adducts (150 nm), evidencing that as the antibody is bounded to long pegylated chains, it retains a non-negligible self-mobility after the functionalization.